High-resolution image of Calaveras Fault seismicity

David P. Schaff,[1] Götz H. R. Bokelmann, and Gregory C. Beroza
Department of Geophysics, Stanford University, Stanford, California, USA

Felix Waldhauser[1] and William L. Ellsworth
U.S. Geological Survey, Menlo Park, California, USA

Received 23 May 2001; revised 14 March 2002; accepted 19 March 2002; published 13 September 2002.

[1] By measuring relative earthquake arrival times using waveform cross correlation and locating earthquakes using the double difference technique, we are able to reduce hypocentral errors by 1 to 2 orders of magnitude over routine locations for nearly 8000 events along a 35-km section of the Calaveras Fault. This represents ~92% of all seismicity since 1984 and includes the rupture zone of the *M* 6.2 1984 Morgan Hill, California, earthquake. The relocated seismicity forms highly organized structures that were previously obscured by location errors. There are abundant repeating earthquake sequences as well as linear clusters of earthquakes. Large voids in seismicity appear with dimensions of kilometers that have been aseismic over the 30-year time interval, suggesting that these portions of the fault are either locked or creeping. The area of greatest slip in the Morgan Hill main shock coincides with the most prominent of these voids, suggesting that this part of the fault may be locked between large earthquakes. We find that the Calaveras Fault at depth is extremely thin, with an average upper bound on fault zone width of 75 m. Given the location error, however, this width is not resolvably different from zero. The relocations reveal active secondary faults, which we use to solve for the stress field in the immediate vicinity of the Calaveras Fault. We find that the maximum compressive stress is at a high angle, only 13° from the fault normal, supporting previous interpretations that this fault is weak. *INDEX TERMS:* 7230 Seismology: Seismicity and seismotectonics; 7209 Seismology: Earthquake dynamics and mechanics; 7294 Seismology: Instruments and techniques; 7205 Seismology: Continental crust (1242); *KEYWORDS:* double difference, correlation, Morgan Hill, earthquake location

Citation: Schaff, D. P., G. H. R. Bokelmann, G. C. Beroza, F. Waldhauser, and W. L. Ellsworth, High-resolution image of Calaveras Fault seismicity, *J. Geophys. Res.*, *107*(B9), 2186, doi:10.1029/2001JB000633, 2002.

1. Introduction

[2] The Calaveras Fault is one of the most active branches of the San Andreas Fault system in northern California (Figure 1). In the 20th century there have been a series of moderate magnitude earthquakes some of which have repeated [*Oppenheimer et al.*, 1990]. The largest of these earthquakes was the *M* 6.2 1984 Morgan Hill earthquake, which appears to have been a repeat of an earthquake in 1911. The long-term slip rate on the Calaveras Fault to the south of where the Hayward Fault splays from it is thought to be 15 ± 3 mm/yr [*Working Group on California Earthquake Probabilities* (*WGCEP*), 1999]. In addition to rupture in moderate earthquakes, this section of the Calaveras Fault has been extraordinarily active in microearthquake activity. It is also known to creep with an average rate of ~13.5 mm/yr since 1997 [*WGCEP*, 1999]. Because of the combination of a fast slip rate, the presence of creep, and equivocal paleoseismic evidence for large earthquakes in the past, the potential for future large earthquakes on the central section of the Calaveras Fault remains uncertain [*WGCEP*, 1999].

[3] *Oppenheimer et al.* [1990] studied microearthquake activity of the Calaveras Fault in great detail. They found a correspondence between the areas that slipped in moderate earthquakes with areas that were relatively devoid of microearthquake activity. They also found that small earthquakes had a very similar spatial distribution both before and after moderate earthquakes. They proposed that the areas devoid of seismicity were stuck between moderate earthquakes and used this assumption to identify two likely source zones for future moderate earthquakes on the Calaveras Fault.

[4] The geometry of fault zones within the Earth is revealed primarily by seismicity. In this study, we greatly improve the earthquake locations on the Calaveras Fault. Our ability to resolve fault zone structure and hence to address many essential aspects of earthquake behavior, is limited by our ability to obtain precise earthquake locations. While quantitative earthquake location techniques date back to the early years of the 20th century [e.g., *Geiger*, 1910],

[1]Now at Lamont-Doherty Earth Observatory, Palisades, New York, USA.

0148-0227/02/2001JB000633$09.00

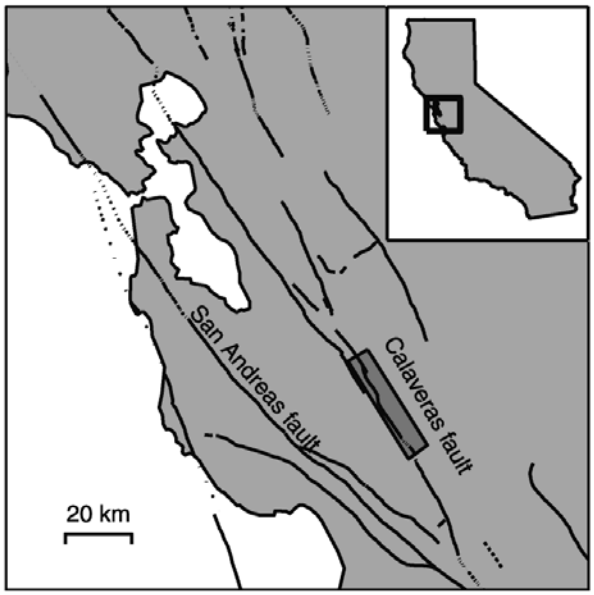

Figure 1. Calaveras Fault in California. Shaded box denotes study area.

our incomplete knowledge of Earth structure and the difficulty of measuring arrival times accurately typically limits the accuracy of earthquake locations to tens of kilometers at teleseismic distances and several kilometers at regional distances even in well instrumented regions like California and Japan.

[5] Uncertainty in earthquake locations can be dramatically reduced by aiming for precision, rather than accuracy, in the form of relative earthquake locations [e.g., *Poupinet et al.*, 1984; *Fréchet*, 1985; *Deichmann and Garcia-Fernandez*, 1992; *Got et al.*, 1994]. In this study, we improve the precision of earthquake locations in two principal ways: (1) removing substantial velocity model error with the double difference approach [*Waldhauser and Ellsworth*, 2000] and (2) reducing relative arrival time measurement errors by waveform cross correlation [*Schaff*, 2001]. The combination allows us to reduce relative location errors by 1 to 2 orders of magnitude for the entire data set.

[6] What emerges from the improved earthquake locations is a highly refined picture of seismicity on the Calaveras Fault. Numerous features that were seen as clouds of seismicity are brought into sharp focus. These features include streaks of earthquakes that are elongated in the direction of slip, sets of repeating microearthquakes that recur up to dozens of times, and large areas of little or no seismicity. We are also able to obtain a much clearer view of a kilometer-scale compressional fault offset and its geometry at depth. Our locations suggest that the two principal offset fault strands may merge near the base of the seismogenic zone. We are also able to resolve secondary fault structures, which were previously suggested by focal mechanisms [*Oppenheimer et al.*, 1988]. Slip on these structures indicate that the maximum compressive stress is at a high angle to the Calaveras Fault implying that it is weak if the stress remains unfavorably oriented on the fault plane. This seems likely, as secondary structures are active to within 100 m of the main fault trace. If the stress rotates into a more favorable orientation, it must do so within the immediate proximity of the fault. The improved locations also allow us to constrain the degree of strain localization on the Calaveras Fault. We find a very narrow fault zone width of no more than 75 m at seismogenic depths.

2. Data and Technique

[7] The waveforms for the event set of 7857 earthquakes comprise over half a million seismograms. They are recorded on Northern California Seismic Network (NCSN) vertical component, short period stations archived at the Northern California Earthquake Data Center (NCEDC). The correlation-double difference method we use scales differently than traditional relative relocation techniques. If only absolute travel times are used the number of observations goes approximately as $N_e \times N_s$, where N_e is number of events and N_s is the number of stations. To do all possible correlations, on the other hand, requires on the order of $N_e(N_e - 1)N_s/2$ measurements. For our study of the Calaveras Fault we have chosen NCSN stations within 70 km, which amounts to on average 50 stations per event. For $\sim$8000 events, this translates to approximately 3 billion possible unique cross correlations for both *P* and *S* waves. The correlation measurements are obtained by a two-step procedure: align to the nearest sample using 2.56 s window lengths and then compute to subsample precision with 1.28 s window lengths [*Schaff*, 2001]. We are able to perform about one million correlation measurements per hour, so total computation time including input/output would amount to approximately half a year.

[8] Differential travel times derived from cross correlation are most accurate for events that occur in close proximity to one another. There are several reasons for this. As the interevent distance increases, waveform similarity decreases and undermines the basis for cross correlation as a means for determining relative arrival times. Moreover, at short interevent distances, differential arrival time measurements allow one to remove nearly all of the common mode error due to unmodeled path effects. As interevent distance increases this no longer holds and the advantage of locating earthquakes using differential arrival times is diminished.

[9] Since the events we consider span a 35-km stretch of the Calaveras Fault, we can significantly reduce the computational time by recognizing that cross-correlation measurements become less useful at increasing interevent distances. In this study we perform correlation measurements only for interevent distances less than 1.5 km in the horizontal and 3 km in the vertical, which limits the number of cross correlations to 108 million ($\sim$3.4% of the total possible measurements). This selection is based both on the magnitude of location errors in the NCSN catalog, and the observation that cross-correlation derived relative arrival times are only an improvement over catalog phase data up to interevent distances of $\sim$2 km for this region [*Schaff*, 2001]. Reducing the number of measurements allowed us to complete the cross correlations in $\sim$1 week.

[10] Of the 108 million relative arrival time measurements, we retain only 8 million (7.5%). We select only those observations that have both normalized cross-correlation coefficients above 70% and mean coherence above 70%. This criterion is based on the observed levels of post-fit

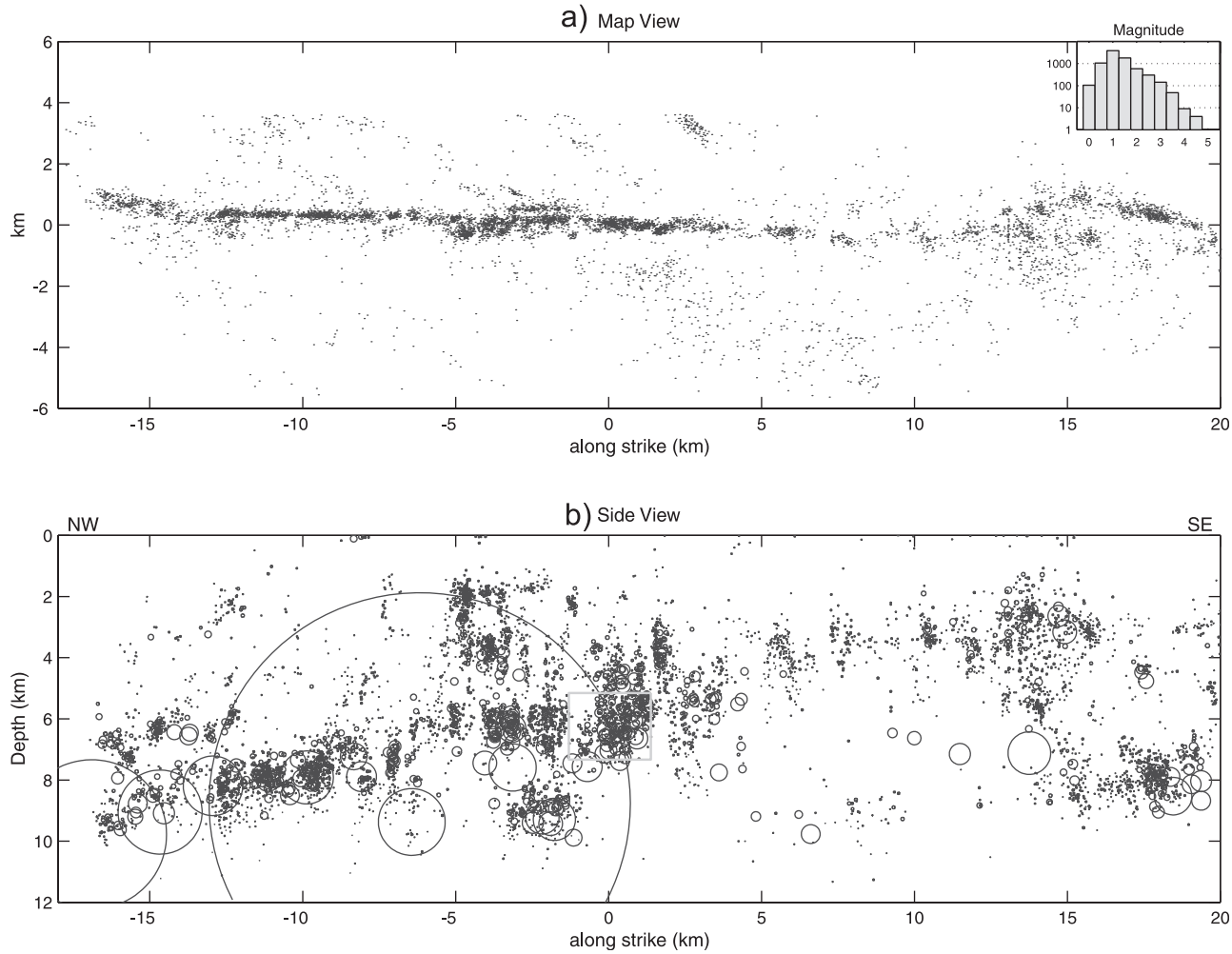

Figure 2. Original catalog earthquake locations recorded by the NCSN for the Calaveras Fault from 1984 through 1997, comprising 7857 events. (top) Map view of events along the Calaveras Fault (146° strike). Inset reveals a Gutenberg-Richter magnitude distribution. (bottom) Fault plane side view displaying only on-fault earthquakes with estimated source sizes based on circular crack model using a 3 MPa stress drop. The largest event is the *M* 6.2 Morgan Hill main shock. Origin is at (37.36, −121.64).

residuals from relocations that included sets of repeating earthquakes [*Schaff*, 2001] and has the effect of removing most of the unreliable measurements from the data set. After applying this cut-off we are left with a data set composed of 4.9 million *P* wave observations and 3.1 million *S* wave observations that are used to estimate hypocentral locations by the double difference technique.

[11] To constrain large scale structures and fill in where there are no good correlation measurements available, we use catalog phase data to form relative arrival time pairs [*Waldhauser and Ellsworth*, 2000]. This adds approximately an additional 1.5 million observations. Interevent distance weighting functions are applied to both catalog and correlation data and are allowed to vary for different iterations in the linearized least squares inversion procedure. It is not known a priori to what separation distances correlation data is reliable. Because of this they are down-weighted with respect to the catalog data (1:100) for the first 10 iterations so as to have minimal effect on the inversion. Using the improved locations, all correlation measurements are subsequently removed for event pairs separated by more than 2 km. The correlation measurements are then weighted more strongly than the catalog data (100:1) to constrain structures at intermediate spatial scales. At iteration 20, correlation data with interevent distances greater than 500 m are removed to further enhance the fine-scale detail [*Waldhauser*, 2001].

[12] One should note that the two data types measure different things. The catalog phase picks on the first break constrain the hypocenter whereas correlation measurements on a windowed wave arrival of some duration will constrain the spatial centroid of moment release. For the majority of these small events, however, the difference between hypocenter and centroid is not resolvable within the errors. For the larger events it may be possible to distinguish the two and hence infer rupture direction [*Waldhauser et al.*, 1999].

3. Relocation Results

[13] Figure 2 shows earthquake locations on the Calaveras Fault from the NCSN catalog in map and side view. Figure 3 displays the same events after relocation. The seismicity

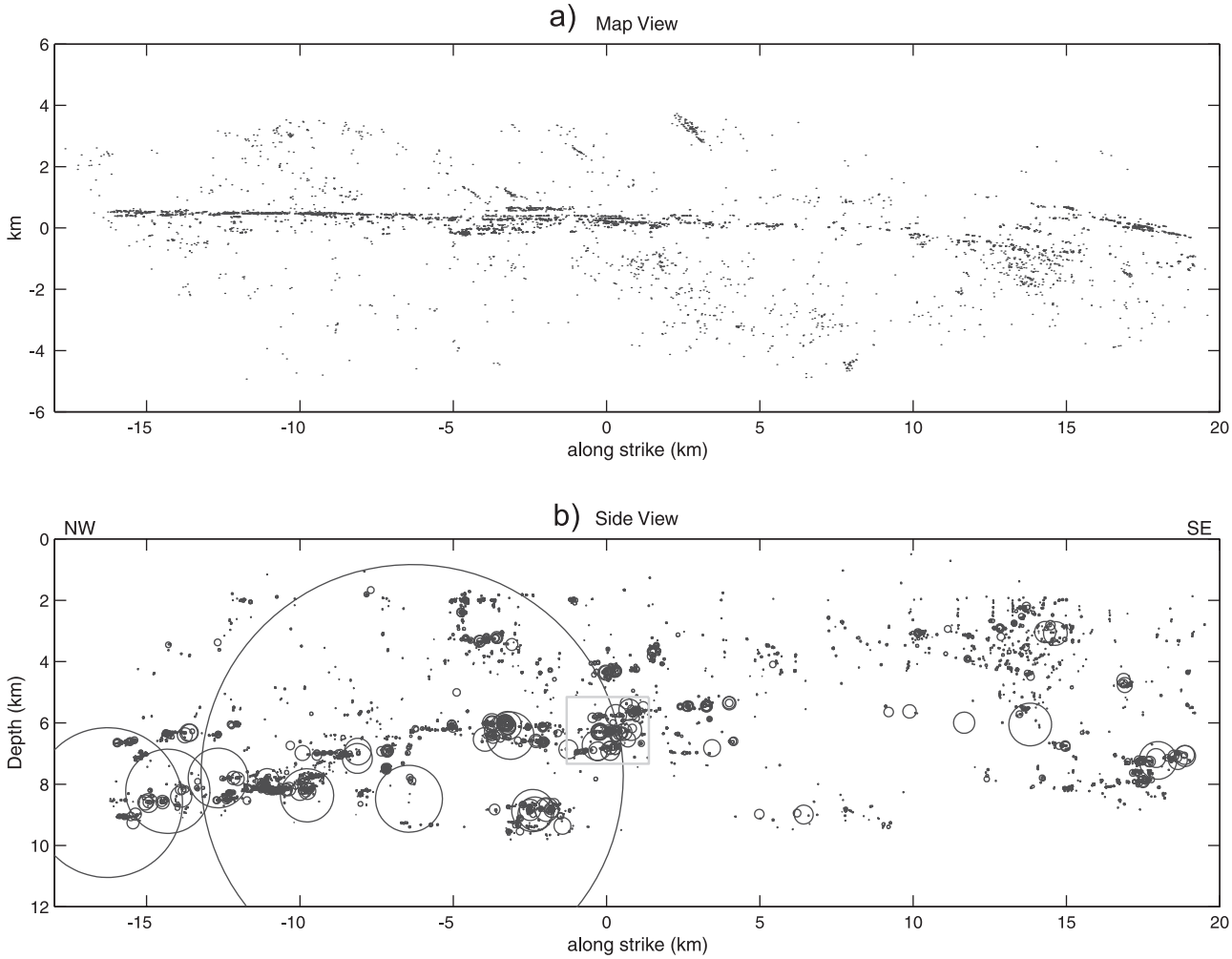

Figure 3. Improved relocations using correlation-double difference technique displaying all 7857 events on same length scale. (a) Note fine scale structure that becomes apparent as well as several off-fault structures now resolved. (b) Substantial improvement of vertical errors concentrates seismicity onto several discrete bands containing events of widely varying magnitudes. Origin is at (37.36,−121.64).

represents 92% of the events for which waveform data is available from 1984 through 1997, a data set that includes the aftershocks of the *M* 6.2 1984 Morgan Hill earthquake. The relocated catalog appears complete down to *M* 1 and is observed to follow a Gutenberg-Richter magnitude distribution. 7724 of the events (98%) are less than *M* 3, 133 are greater than or equal to *M* 3. Off-fault events were removed from Figures 2b and 3b in side view. Upon relocation, the seismicity becomes highly clustered. It is clear from the comparison that catalog location errors, particularly in hypocentral depths, obscure much of the underlying structure.

[14] Formal errors in the catalog hypocenters for this region give average 95% confidence estimates of 1.2 km in the horizontal and 2.5 km in the vertical. Relative errors in the relocated catalog strongly depend on the precision of the data used and the separation between the events. Location errors are typically one to two orders of magnitude smaller compared to the catalog data. Bootstrap residual analysis indicates that highly correlated events in repeating earthquake sources and streaks have errors in the range of meters to a few tens of meters [*Waldhauser and Ellsworth*, 2000]. These errors most likely reflect fine-scale precision controlled by the correlation data. Uncorrelated events located with phase picks have relative errors between several tens of meters to a few hundreds of meters. Single error estimates attached to individual earthquakes do not adequately describe the location precision on different length scales. For instance, larger features will have correspondingly higher relative location errors due to the introduction of model errors. *Rubin* [2002] has relocated an overlapping portion of the Calaveras Fault and obtains locations that are in good agreement with ours within the error estimates described above. A comprehensive, quantitative analysis of these relative errors has not been fully developed and is beyond the scope of this paper.

[15] The degree to which seismicity coalesces onto discrete structures can be better appreciated by magnifying a small area on the fault. Figure 4 shows the effect of relocation on the organization of seismicity on the small scale. The diffuse arrangement of locations characteristic of the initial catalog locations becomes highly clustered. Many smaller events appear to nucleate at the boundaries of larger events, suggesting that they represent failure of stress concentrations at the edges of the larger earthquakes [*Ellsworth*,

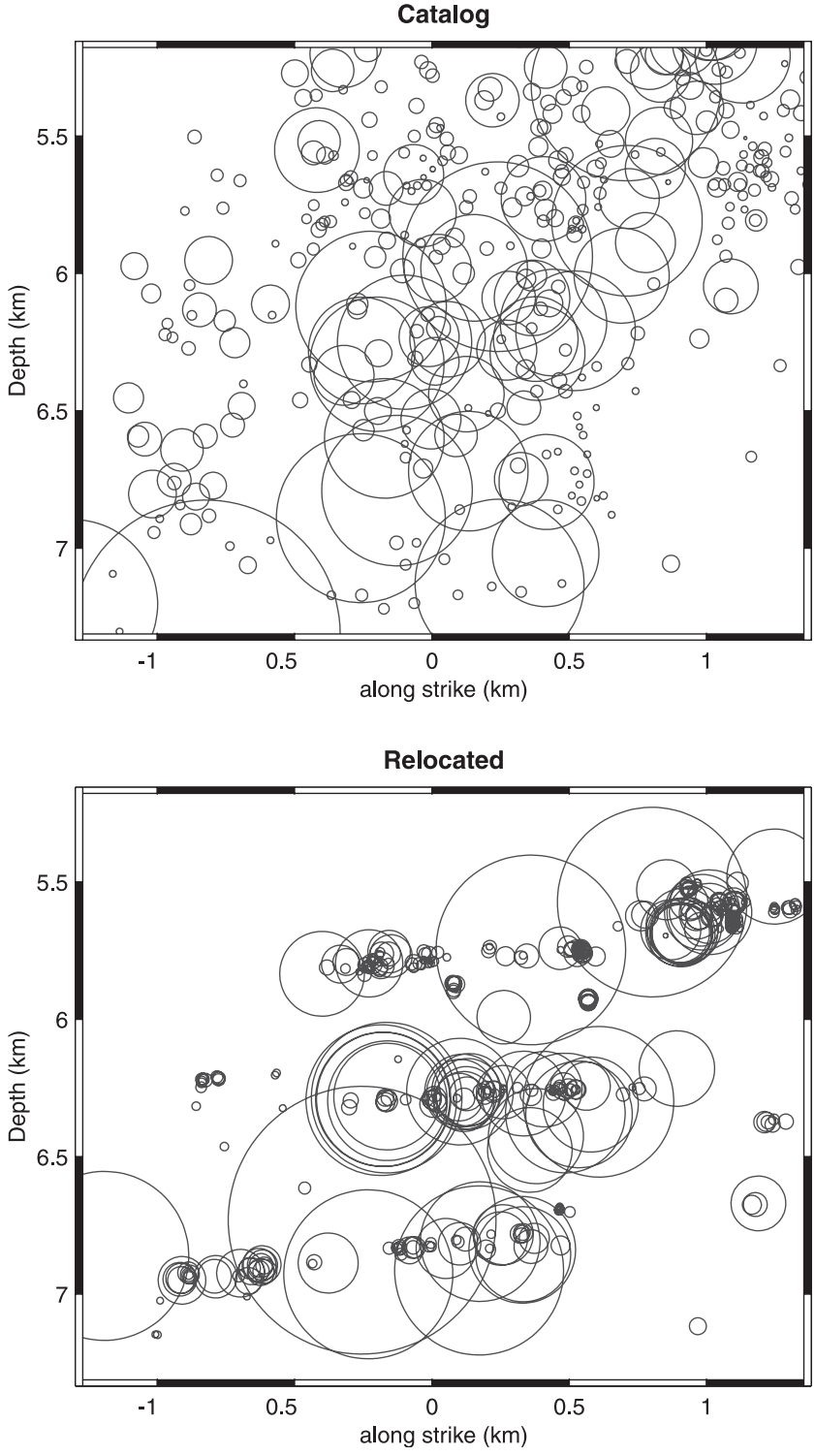

Figure 4. Zoom plots of the seismicity contained within the gray boxes on Figures 2 and 3.

1995; *Rubin et al.*, 1999]. This feature is also seen later in Figure 7b.

[16] It is evident from the side view in Figure 3 that events of widely varying magnitudes fall onto prominent linear structures. Similar streaks of seismicity have been observed on the San Andreas and Hayward Faults [*Rubin et al.*, 1999; *Waldhauser et al.*, 1999]. On other parts of the fault there is little or no seismicity. This pattern was recognized for the Calaveras Fault by *Oppenheimer et al.* [1990], who noted that moderate earthquakes on the Calaveras Fault tend to occur in these holes in seismicity. After relocation, the uneven distribution of seismicity on the fault becomes even more dramatic.

[17] Surprisingly, the seismogenic part of the fault zone does not penetrate below 10 km depth in Figure 3. It is possible that the lowermost events from −15 to −9 km

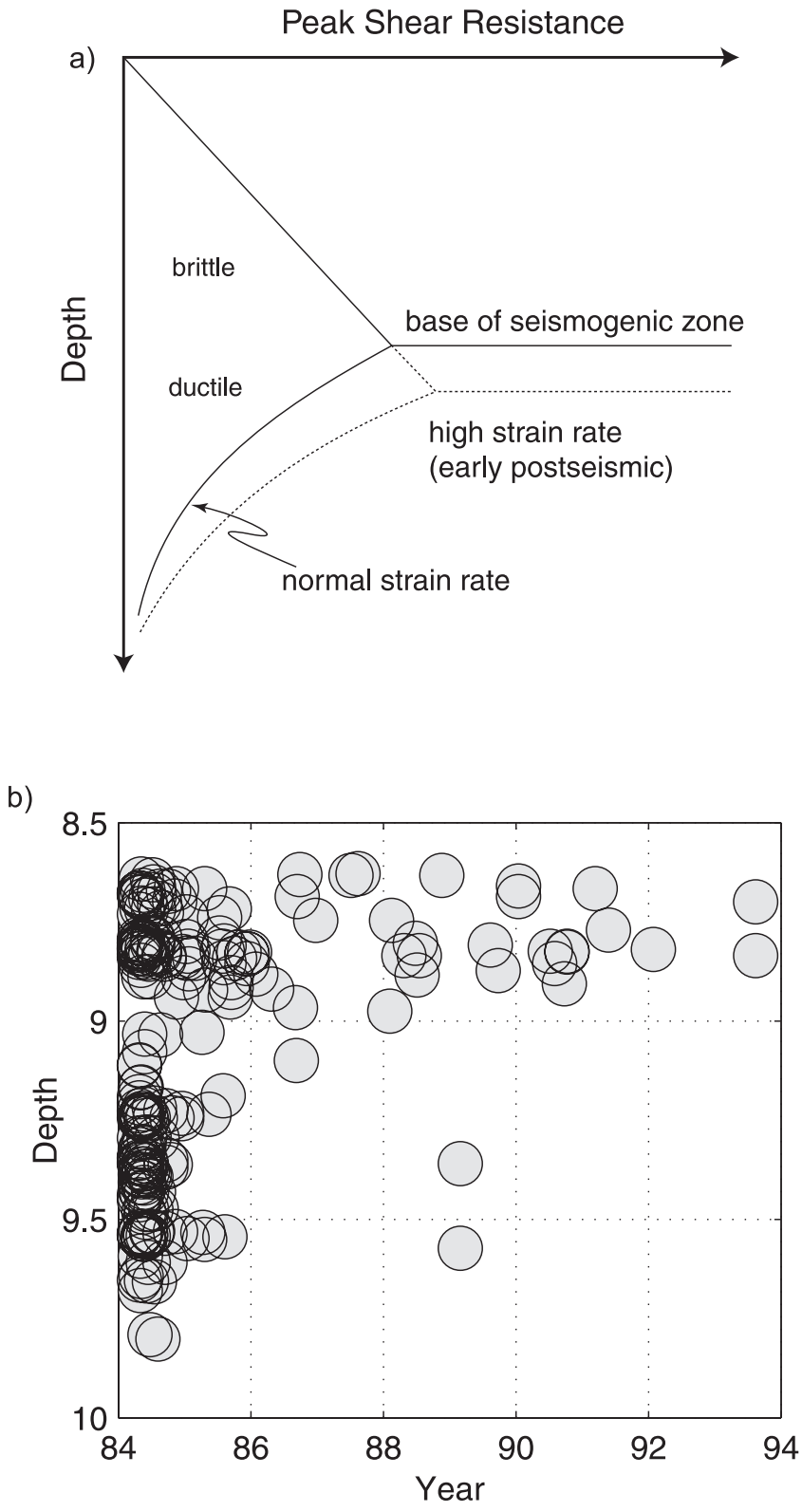

Figure 5. (top) Cartoon depicting change of brittle-ductile transition due to higher strain rates right after the main shock. (bottom) Temporary existence of deeper events is consistent with above mechanism.

along strike distance occur at the brittle-ductile transition. The depth of this transition will depend on strain rate [*Sibson*, 1984]. Figure 5a illustrates that the depth of the brittle-ductile transition might increase due to the higher strain rates immediately following the 1984 Morgan Hill main shock. Figure 5b displays evidence consistent with this mechanism. Plotted are events between 8.5 and 10 km depth at -2 km along strike (Figure 3) as a function of

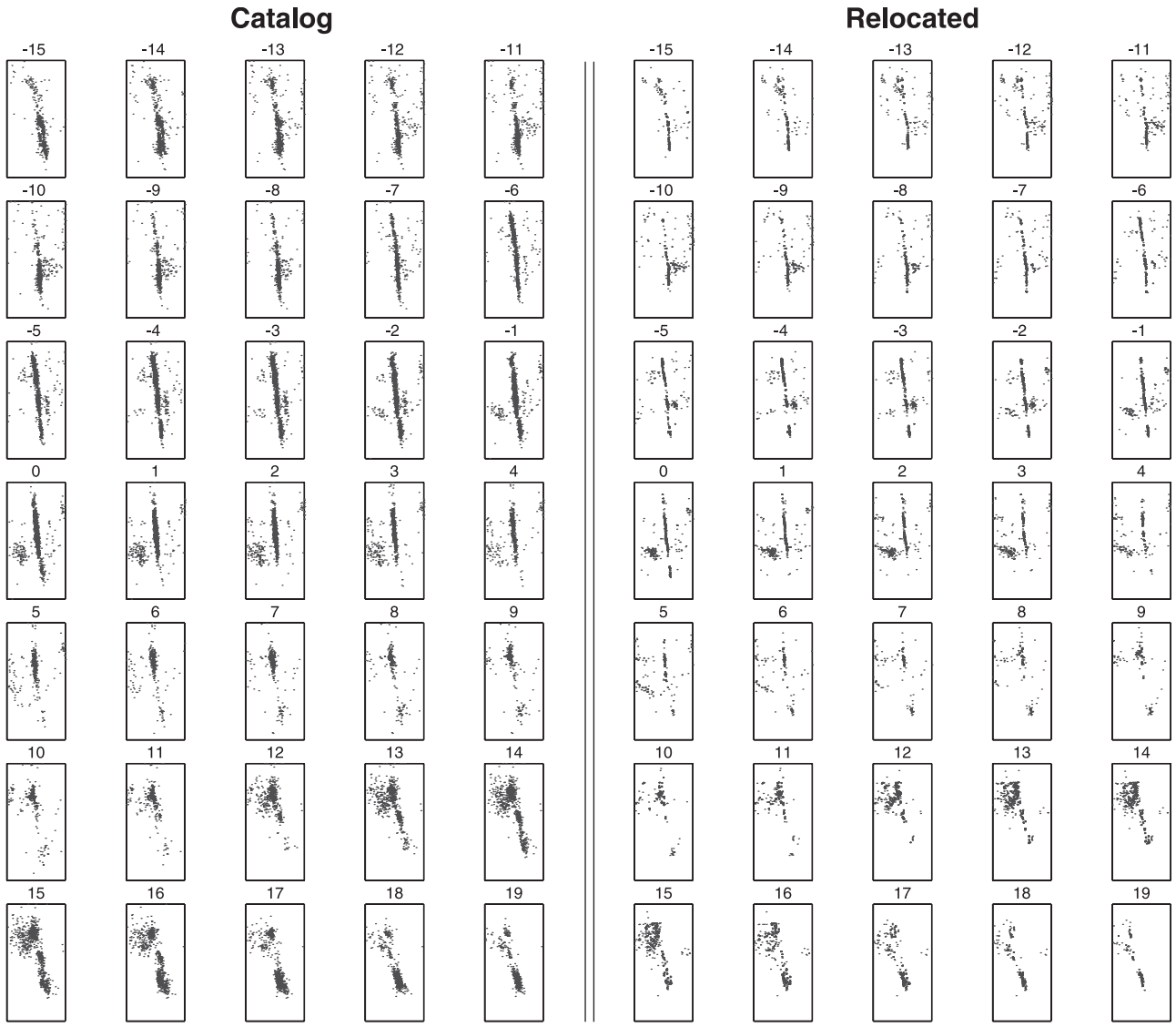

Figure 6. Cross-sectional views looking to the NW for (left) catalog locations and (right) relocated seismicity. Boxes are 6 km across fault and 12 km in depth and span 4 km along the fault. Numbered center of each box corresponds to distance along strike in Figures 2 and 3.

origin time. We observe that the ~100 events below 9.1 km follow a steep Omori's law but only occur in the immediate postseismic period up to 1986. The shallower events on the other hand also follow Omori's law but persist until 1994. Thus it is possible that the base of the seismogenic zone normally occurs around 9 km depth in this area, but temporarily increases more than 500 m deeper due to the increased strain rates after the Morgan Hill main shock. The interpretation is not conclusive since the phenomenon is only observed on a small portion of the fault and not under other high slip areas. Assuming hydrostatic pore pressure together with representative values of the geothermal gradient and strain rate, an increase in the depth of the brittle-ductile transition of ~1 km corresponds to an increase in the strain rate of approximately a factor of 10 [*Sibson*, 1984].

[18] Figure 6 shows latitudinal cross sections of seismicity, i.e., cross sections oriented perpendicular to the strike of the Calaveras Fault, before and after relocation. Clearly the Calaveras Fault as expressed by seismicity at depth is extremely thin. Parts of the fault that appear in map view to have substantial width, e.g., from −5 to 0 km along strike, are seen in cross section to be an apparent width from the surface projection of a dipping planar fault. Only in areas where the depth extent of seismicity is small or where the fault plane is more vertical, does the fault appear narrow in map view.

[19] Several previously obscured planar distributions of seismicity are now apparent as well. These include several vertical N-S trending faults to the north and east of the Calaveras Fault (Figure 3). The broad region of seismicity to the west of the Calaveras between 0 and 10 km along strike is seen in cross section to form a blind thrust fault parallel to and southwest of the Calaveras Fault that dips ~30 to the northeast (Figure 6). This seismicity does not appear to match any mapped fault traces when extrapolated to the surface. As will be shown later, the focal mechanisms

for events on these off-fault structures are consistent with the alignment of hypocenters and confirm the orientation of these subsidiary faults. Most of the off-fault seismicity appears to be influenced by the Morgan Hill main shock and is observed to follow Omori's law of aftershock decay.

4. Streaks

[20] A number of linear features are apparent in the seismicity plot of Figure 3. These streaks of seismicity are predominantly horizontal, which coincide with the right-lateral slip direction on the Calaveras Fault. Similar alignments of seismicity have been observed on the San Andreas and Hayward Faults and in the southeast rift zone at Kilauea, Hawaii [*Gillard et al.*, 1996; *Rubin et al.*, 1999; *Waldhauser et al.*, 1999; *Waldhauser and Ellsworth*, 2002]. In each of these cases the streaks appear closely aligned with the slip direction on the fault, suggesting that the streaks arise due to a slip-controlled process rather than something else such as horizontal layering [*Rubin et al.*, 1999; *Waldhauser et al.*, 1999; *Waldhauser and Ellsworth*, 2002]. For the Calaveras Fault we find that while many of the streaks are nearly horizontal, some appear to have a slight dip (Figures 3 and 4).

[21] Figure 7 shows two of the streaks on the Calaveras Fault in detail. The first is a 2-km subhorizontal streak that occurs around −10 km along strike distance on Figure 3 and is composed of many events of variable magnitude with significant spatial overlap. The four $M \sim 3$ between 0 and 0.5 km in Figure 7 appear to bridge the gap in the streak between the two strands composed of smaller events. Figure 7c is analogous to plots made by paleoseismologists with the inferred rupture length along strike for each event versus calendar time. Figure 7c shows no clear recurrence pattern other than the tendency for events on adjacent fault segments to be correlated in time. There is significant overlap of seismicity within the streak, and the range of observed magnitudes is more or less continuous as demonstrated in Figure 7e.

[22] The second streak detailed in Figure 7 is located at −4 km on Figure 3. Events on this streak also have a wide range of magnitudes. Smaller events tend to occur on the periphery of larger earthquakes. In this streak, however, the seismicity is composed largely of repeating earthquakes. The overlapping circles of similar size indicate that parts of the fault rupture repeatedly in the same sized earthquakes. Figure 7f shows that there are characteristic magnitudes which correspond to those of the repeating events. In contrast, the magnitude distribution over the entire fault in Figure 2 obeys the classic Gutenberg-Richter relation, (100 *M* 3, 10 *M* 4, 1 *M* 5). The recurrence interval is also more regular in time and not as strongly correlated with the timing of earthquakes in adjacent segments. These observations suggest that the locked patches of the fault that fail in stick-slip are more isolated on this streak compared with the first streak. The relative isolation of slipping patches could more easily lead to reestablishing the same initial conditions at the onset of earthquakes and hence would lead to reoccurrence of characteristic earthquakes. The relative isolation would also lead to weaker interaction of adjacent earthquakes and hence a more regular recurrence interval.

[23] Many of the events in our study can be considered aftershocks of the 1984 Morgan Hill, California, earthquake. The repeating earthquake sequence at 0.5 km in Figure 7d is an example of a repeating earthquake sequence that follows Omori's law of aftershock decay. *Schaff et al.* [1998] showed that repeating aftershocks of the 1989 Loma Prieta also followed Omori's law. They also demonstrated that this observation is consistent with loading of a stuck patch on an otherwise creeping fault in response to a stress step, where the creeping part of the fault obeys a steady state velocity strengthening friction law. In this case the stress step would have been provided by the 1984 Morgan Hill, California, earthquake. It is interesting to note that the occurrence of ∼13 *M* 3.3 earthquakes 500 m away from this repeating sequence does not appear to influence the timing of these events.

[24] Assuming a constant stress drop of 3 MPa and a circular crack model, an estimate of the slip for each event can be made. Figures 7g and 7h display cumulative slip isochrons plotted for the occurrence of each event within the streak. The characteristic, more predictable behavior, clearly emerges again for the second streak on the right. The two clusters at 0.5 km and 1 km appear to have similar slip rates over the ∼15-year interval, despite the difference in magnitudes (1.7 and 2.6, respectively). The cluster of magnitude 3.3, however, would correspond to over 5 times this slip rate for the same time period, given the assumption of a constant stress drop. An intriguing feature can be found by the arrow at −0.7 km, where two clusters of different magnitudes rupture the same fault patch with interwoven recurrence intervals. If we assume that the smaller of these events is set up repeatedly with the same initial conditions between large events, then it suggest that much of the area that slips in the larger events may also slip aseismically [*Beeler et al.*, 2001].

[25] Surprisingly, the first streak appears to display some systematic behavior in the accumulation of slip along strike compared to the absence of regular recurrence intervals or repeated hypocentral locations from Figures 7a and 7b. A somewhat uniform slip rate across this streak results from our assumptions. Applying a linear stress drop with moment relation after [*Nadeau and Johnson*, 1998] and [*Nadeau and McEvilly*, 1999] produces a more irregular slip distribution and a rather large 2 m of cumulative slip for the *M* 3.3 in the second streak. It will be difficult for any simple stress drop scaling to satisfy a uniform slip rate. There are approximately the same number of the *M* 1.7 and *M* 3.3 events (16 and 13, respectively) and only five *M* 2.6 events. Thus any constant or monotonically changing stress drop with earthquake size will not result in uniform slip.

[26] If a rectangular source is assumed where the length is greater than the height, it will smooth out the slip distribution compared to that for the circular crack model. With an aspect ratio of 3:1 or larger, the slip is relatively uniform, but many of the fault segments rupture repeatedly both as large and small events. Although, the regular recurrence of the *M* 1.7 events suggests that this is not occurring.

[27] For seismic slip on circular asperities to keep pace with the surrounding creep rate, unusually high stress drops are implied [*Nadeau and Johnson*, 1998; *Nadeau and McEvilly*, 1999]. A model where repeating earthquakes occur at the border between creeping and locked zones

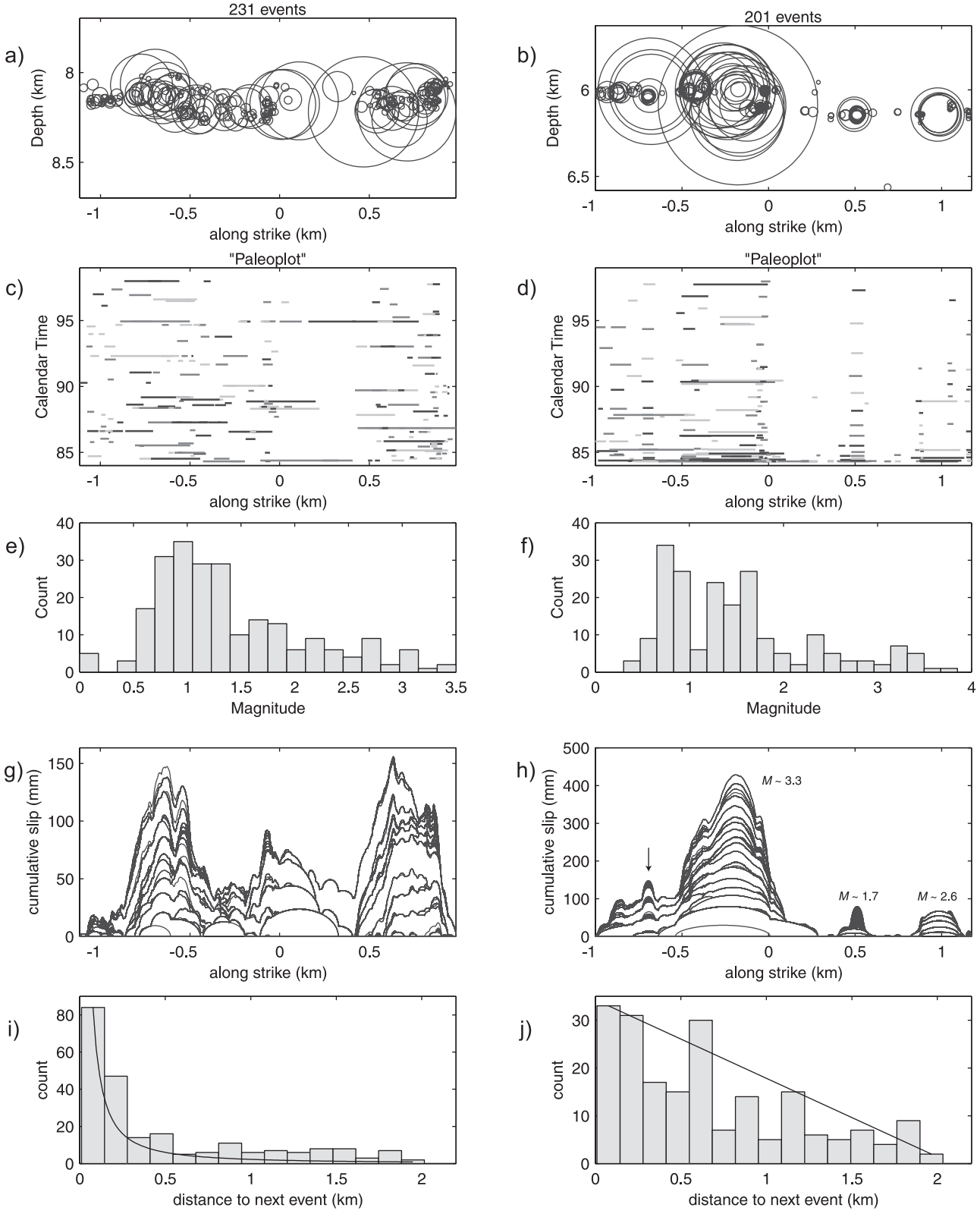

Figure 7. Comparison of two linear structures for characteristic-type features in space, time, and size. (left) A 2 km long streak consisting of a continuous range of several magnitudes. No clear discernible pattern is observed in time. Evidence of earthquake triggering is present in Figure 7i. (right) Aligned multiplets which contain events of discrete magnitudes, repeatable hypocenters, and many recurrence intervals that can be predicted by an Omori-type decay. These recurrence intervals seem largely unaffected by neighboring events and represent minimal earthquake interaction. See text for more detailed explanation.

Table 1. Statistics for 7409 Relocated Events[a]

Distance, m	15 years	1 day	1 min
	Relocated Catalog		
100	5930 (80%)	573 (7.7%)	71 (1.0%)
50	5560 (75%)	320 (4.3%)	43 (0.6%)
25	4890 (66%)	118 (1.6%)	20 (0.3%)
10	3186 (43%)	21 (0.3%)	4 (0.1%)
	Simulated Catalog		
100	3563 (48%)	16 (0.2%)	0 (0%)
50	848 (11%)	4 (0.1%)	0 (0%)
25	110 (1.5%)	0 (0%)	0 (0%)
10	6 (0.1%)	0 (0%)	0 (0%)

[a] The simulated catalog is random in space but with the same time distribution as the relocated catalog.

produces the common lower stress drops ($\sim$1 MPa), which are constant for all magnitudes [*Sammis and Rice*, 2001]. The distribution of streaks with multiple parallel strands in Figure 4, however, seems incompatible with a simple boundary between creeping and locked zones.

[28] From the surface creep rate of 15 mm/yr an estimated 225 mm could have accumulated over this time span, a value approached only at a few places along the streaks. The repeating earthquake models can be divided into two classes based on how they account for total slip across the asperity: either as the sum of aseismic and seismic slip [*Beeler et al.*, 2001] or seismically [*Nadeau and Johnson*, 1998; *Sammis and Rice*, 2001]. On the 2 km scale of these streaks with clusters of repeating events in such close proximity, it may be reasonable to assume a uniform loading rate across the asperities. Yet the choice of a constant or variable stress drop produces fairly irregular cumulative slip distributions with significant gaps. This suggests that a uniform geodetically determined slip rate cannot entirely be accounted for seismically but that aseismic processes contribute substantially to the deformation as well [*Bakun et al.*, 1986; *Beeler et al.*, 2001].

[29] Figures 7i and 7j display a marked difference in earthquake interaction between the two streaks. For the first streak a large number of events occur in close proximity to the one that happened just before it, suggesting strong earthquake interaction. In other words, events are tending to trigger rupture on adjacent fault segments. For the second streak the linear fall-off is what would be expected for purely random spatial and temporal behavior in the absence of earthquake interaction. This observation fits cleanly with our idea on the necessary conditions in order for repeating clusters of events to occur: isolated stuck patches, embedded in a sea of creep, whose recurrence intervals are not influenced by surrounding events.

[30] Table 1 attempts to quantify how many of the relocated events are repeats and how many are triggered. The "15 year" column displays the number and percentage of events that have at least one other event over the 15-year interval that occurs within the corresponding distance for that row. The "1 day" and "1 min" columns indicate the number of those event pairs that occur with much smaller time intervals. Therefore at least two thirds (66%) of the events could most likely be classified as repeats because they have at least one other event which occurs within 25 m in the data set. For comparison, Table 1 also shows the statistics if the 7409 events occur randomly over the fault volume in space. The same empirical time distribution of background seismicity plus Morgan Hill aftershocks was used. Note that now only 1.5% of the events could be classified as repeats at the 25-m level for this scenario. An estimated source radius for a M 1.5 event is around 30 m. Hypocenters of larger events can be separated by more and still have significant source area overlap. Approximately 8% (573 events in Table 1 of all the relocated events on the Calaveras Fault appear to be triggered (occurring within 100 m and 1 day from a prior event). Some of the recurrence intervals are extremely short. For example, one pair of events out of the 20 that are within 25 m and 1 min of each other corresponds to a magnitude 2.5 and 2.7 that occurred only 15 s apart in 1988.

5. Holes

[31] There are a number of areas on the Calaveras Fault that have very little microearthquake activity. The filled areas of all the black circles (excluding Morgan Hill) on Figure 8 comprise only $\sim$6% of the total fault area. In other words, 94% of the seismogenic zone in this region has been free of microearthquake activity over the past 15 years. These holes in the seismicity are evident in Figure 8: one from -5 to 1 km along strike and $2-6$ km depth and another at $4-7$ km along strike and at similar depth. The most prominent is the notable absence of seismicity from $10-19$ km along strike at depths greater than 5 km. For the time period considered, these areas have remarkably little earthquake activity when compared with the rest of the Calaveras Fault. Since the Calaveras Fault is known to have both earthquakes as large as M 6.2 and to have a great deal of aseismic creep, it is natural to ask the question of how these holes behave over the long term. Do they slip aseismically or do they slip in moderate earthquakes?

[32] There is direct evidence that at least some of them slip in larger earthquakes. Figure 8 also shows a slip model of the 1984 Morgan Hill earthquake derived from waveform modeling of strong motion data [*Beroza and Spudich*, 1988] together with the relocated seismicity. Although the spatial resolution of main shock slip, particularly the vertical location is poor, it is clear that the area of highest slip in the main shock at approximately +15 km along strike, is situated within the most prominent hole in microearthquake activity. The other area of substantial slip in the earthquake was near the main shock hypocenter at 0 km along strike and 8 km depth, which is located below one of the holes in microearthquake activity. This anticorrelation of main shock slip and earthquake activity has been noted previously [*Hartzell and Heaton*, 1986; *Mendoza and Hartzell*, 1988; *Oppenheimer et al.*, 1990]; however, the degree to which areas of slip in moderate earthquakes are devoid of microearthquake activity in the interim is even more striking after relocation.

[33] It has long been recognized that aftershocks are likely to occur in regions of high main shock-induced stress concentration [e.g., *Beroza and Spudich*, 1988; *Mendoza and Hartzell*, 1988]. It is worth noting, however, that the anticorrelation between microearthquake seismicity and slip in occasional larger earthquakes persists long after aftershock activity has ceased [*Oppenheimer et al.*, 1990]. That is, the seismicity holes are longer-lived features than would

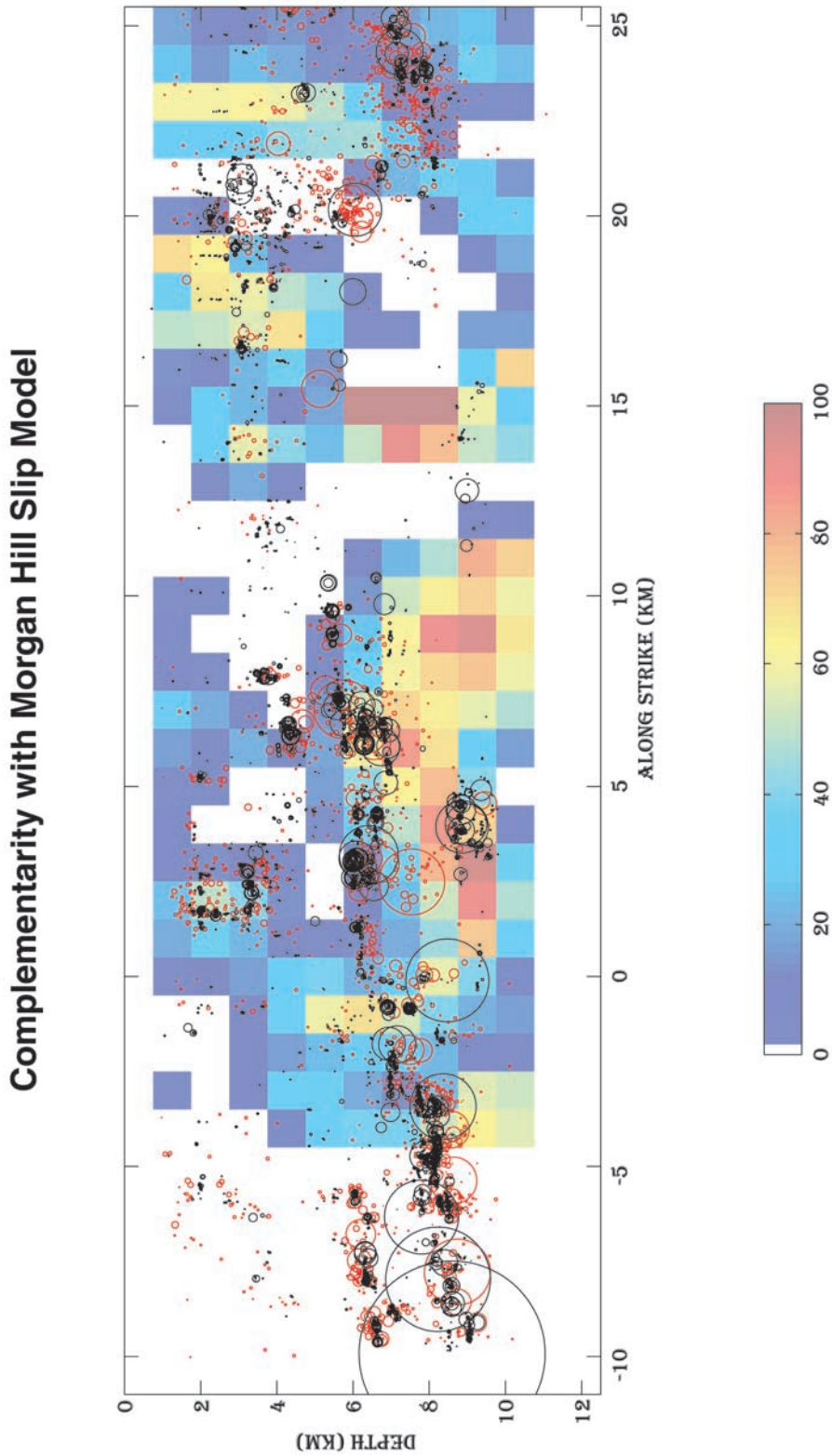

Figure 8. The Morgan Hill slip model [*Beroza and Spudich*, 1988] for the *M* 6.2 event occurring in 1984, compared to the seismicity distribution from 1967 to 1984 (red) and from 1984 through 1997 (black).

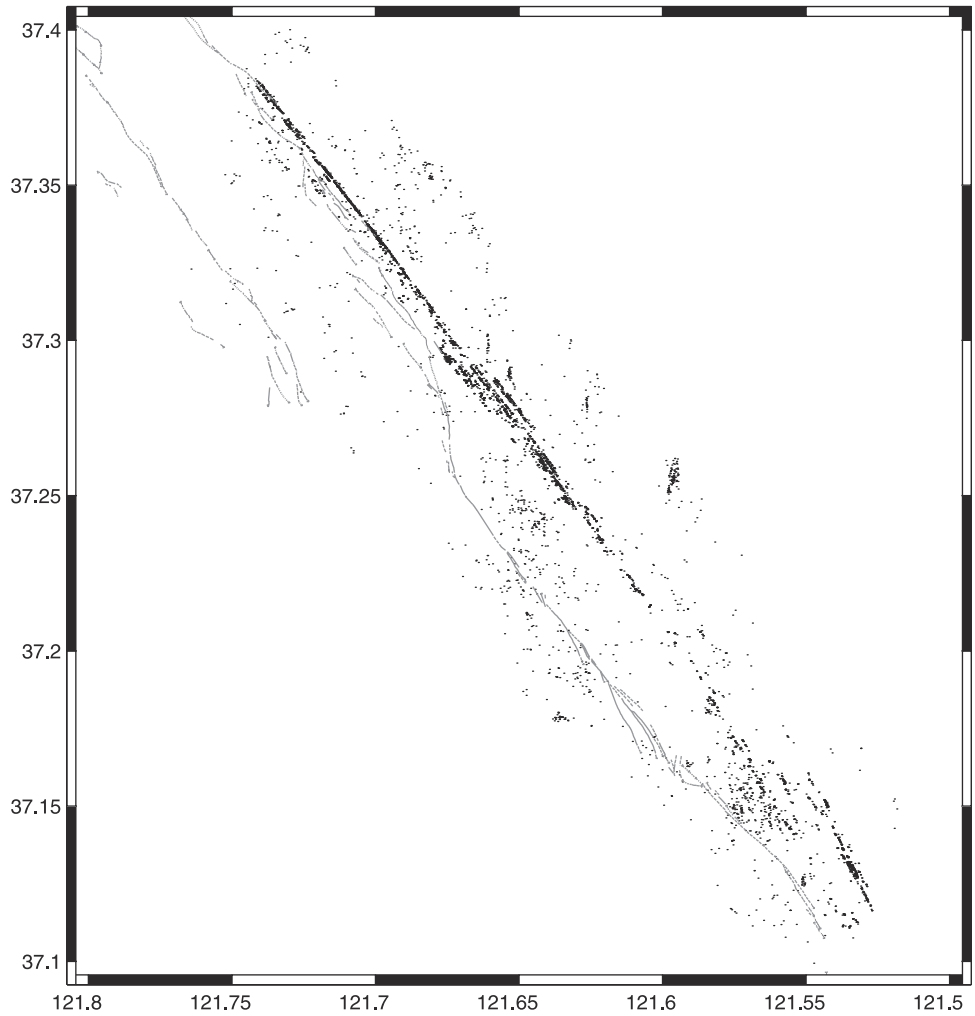

Figure 9. Comparison of relocated seismicity in map view with surface faulting.

be expected if they were simply the byproduct of main shock-aftershock interaction. It was also a preexisting condition. Plotted in red on Figure 8 are pre-Morgan Hill events since 1967, relocated using only catalog phase data. Although the locations are not as precise, the same general pattern of seismicity persists through the main shock. This suggests that stress accumulation and release on the Calaveras Fault is strongly influenced by spatial variations in fault zone properties.

[34] There is indirect evidence that the holes may behave aseismically as well. Slip in the 1984 Morgan Hill earthquake, although complementary to microearthquake activity, does not nearly fill all the aseismic areas (Figure 8). One should note that microseismicity represents very little total slip relative to the main shock. A plausible model for how repeating earthquakes occur is that they are stuck asperities surrounded by creep. There are also holes in seismicity that have not yet been filled with larger earthquakes. Finally, there is geodetic evidence for a very large post-main shock aseismic transient following the 1984 Morgan Hill, California, earthquake [*Prescott et al.*, 1984]. Although the slip is not well located, *Prescott et al.* [1984] presented evidence that it was shallower than most of the main shock slip. Thus it is possible that some of the holes in seismicity are filled with aseismic slip following the 1984 earthquake.

6. A Fault Discontinuity

[35] Maps of the surface trace of the Calaveras Fault display substantially more complexity than suggested by the seismicity at depth. Figure 9 shows that the simple structure with depth does not closely correlate with mapped surface traces. While Figures 3 and 6 indicate that the strike of the Calaveras Fault remains essentially constant from −17 to 8 km along strike with minor fluctuations in dip, the surface expression is more complicated and is unmapped over some stretches. The surface intersection of the dipping seismicity does not coincide with the Calaveras Fault trace, again suggesting a complex relationship between the fault structure at the surface and at depth [*Michael*, 1988].

[36] The events between 8 and 20 km along strike in Figure 3 correspond to panels 10 to 19 on Figure 6. Here the fault structure deviates significantly from a simple planar geometry. In Figure 3, it is evident that these events form a prominent left-stepping fault jog. This will act as a restraining feature for right-lateral slip on the Calaveras Fault. Thus it is likely that this fault segmentation acted to terminate

rupture of the 1984 Morgan Hill earthquake to the southeast. This possibility had been recognized previously [*Bakun et al.*, 1984; *Beroza and Spudich*, 1988]; however, the fault trace at the surface and at depth do not correspond very closely and it was not necessarily clear from the seismicity what the depth extent of the fault offset was. From the relocated seismicity it is clear that the fault discontinuity extends over the same range as slip in the main shock.

[37] Both the surface trace and the relocated seismicity at depth indicate a compressional fault offset of the Calaveras Fault in the southern reaches of our study area; however, the structure of this feature is quite different in the two cases. The geologically mapped surface trace appears quite complicated in the vicinity of the fault offset with multiple parallel strands [*Radbruch-Hall*, 1974]. The fault offset in the surface trace is not located in the same place as the fault offset recorded by microearthquake activity. The seismicity, on the other hand, shows that the offset at depth is on the order of a kilometer, and while there is considerable seismicity off the main fault trace of the Calaveras to the southwest of the jog, most of the seismicity is concentrated on two main fault traces. The western trace appears to dip toward the eastern trace and there is a suggestion that the two meet near the base of the seismogenic zone in the latitudinal cross sections 11–17 of Figure 6. In studies of relocated seismicity near a dilational fault offset at Landers, *Felzer and Beroza* [1999] found no evidence that the two fault traces merged at depth.

[38] It is interesting that our technique appears to do well at refining earthquake locations within and surrounding a fault jog. It is easy to understand why it would work well on a simple planar fault, such as the Calaveras Fault to the northwest of the fault jog. In that area there are abundant microearthquakes and their mechanisms are likely to be essentially identical. A fault jog, however, is inherently three-dimensional and mechanisms will almost certainly be strongly variable. The fact that we get such a clear image of the three-dimensional structure of the fault jog in this case suggests that we can apply these relocation techniques to great effect in areas where structure is quite complicated.

7. Fault Zone Width

[39] One of the most important parameters for understanding both how faults evolve and the mechanics of earthquake rupture is fault zone width. Some measure of fault zone width can be extracted from Figure 6, which shows cross sections of seismicity oriented perpendicular to the fault strike. With the exception of the aforementioned fault discontinuity, nearly all of the earthquake activity defines a very narrow planar zone following relocation. The orientation varies from nearly vertical in the north from -17 to -9 km along strike to a dip to the east of $\sim 85^\circ$ from -5 to 4. Most of the off-fault seismicity clearly falls on other planar structures with different orientations, such as the off-fault blind thrust from 0 to 3 km along strike.

[40] To quantify fault zone width, we divide the fault using a 1 km square grid and measure distance orthogonal to the fault for each event. We then subtract the mean in each box and take 4 times the standard deviation of the estimate. This means $\sim$95% of the relocated earthquakes fall within a planar feature of that width. Figure 10 indicates an average 75-m fault zone width for the Calaveras Fault. For comparison, the widths of the two streaks in Figure 7 are $\sim$25 m. Because the widths we measure are comparable to location errors on these different scales, it is likely that the fault zone is substantially thinner. Our results are consistent with a fault that has zero resolvable width. We also find no evidence for any systematic variation of fault zone width with depth or distance along strike.

[41] Other geophysical estimates of fault width can be obtained by modeling fault zone guided waves. Modeling dispersive wave trains of microearthquakes at Parkfield implies a low-velocity channel 100 to 150 m wide on the San Andreas Fault [*Li et al.*, 1990]. Results for other faults include 100–200 m for Landers [*Li et al.*, 1994], 30–60 m for Kobe [*Li et al.*, 1998], and 120 m for the San Jacinto fault zone [*Li et al.*, 1997]. Comparison with our estimates may in part represent variations in width for different faults. The two measurements provide complementary information. The distribution of earthquakes indicates the part of the fault zone that is currently active, seismically, whereas waveguides delineate a low velocity zone in comparison with the country rock.

8. Stress Orientation

[42] As noted earlier, focal mechanisms of the off-fault seismicity provide independent evidence substantiating the orientation of the structures resolved by the relocation. Figure 11a displays composite focal mechanisms for two N-S trending faults, the blind thrust fault, and events on the Calaveras Fault. The N-S trending faults together with the Calaveras Fault might appear to form a conjugate set. The focal mechanisms of these events, however, clearly show that these faults are not a conjugate set because the mechanisms of events on the Calaveras Fault and on the N-S trending faults are all right-lateral.

[43] The stress tensor orientation based on focal mechanisms and other stress indicators suggests that the San Andreas Fault system is weak in the sense that it slips at a low level of resolved shear traction [*Zoback et al.*, 1987; *Townend and Zoback*, 2001]. The focal mechanisms and off-fault seismicity provide an opportunity to estimate the regional stress in the vicinity of the Calaveras Fault. There are several particularly fortunate aspects to the location and nature of this seismicity for this purpose. There are both right-lateral, strike-slip, and reverse faulting mechanisms with differing orientations compared to the right-lateral strike-slip on the Calaveras Fault. Moreover, for each of these structures the clearly resolved geometry of the seismicity allows us to differentiate the fault versus auxiliary plane ambiguity of the focal mechanism. Finally, the active features reach within a few hundred meters of the Calaveras Fault itself, allowing us to constrain the stress tensor in very close proximity to this major active fault.

[44] We estimate the stress tensor using a method similar to *Angelier* [1979] in which the slip vector and fault plane are both known. The geometry of the active faults and the orientation of the maximum compressive stress are shown

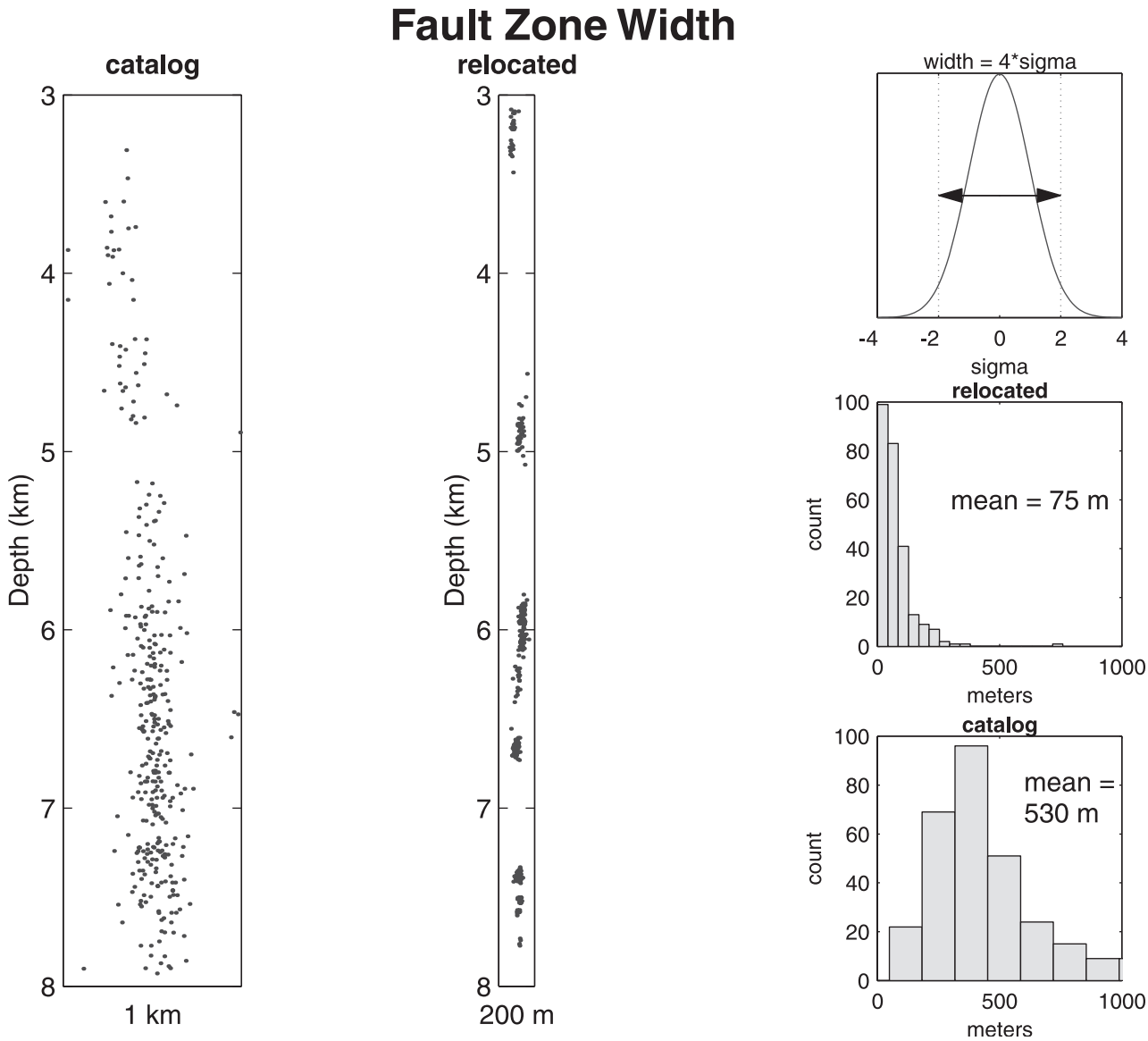

Figure 10. Comparison of improved estimates for fault zone width from original catalog locations and relocations.

in Figure 11. Table 2 shows the data based on the resolved fault geometry that is used to constrain the stress tensor. The two N-S trending faults reach to within ~100 m (N-S1) and 2 km (N-S2) of the fault, respectively. The thrust fault reaches to within <1 km of the main Calaveras Fault as well.

[45] In order for all of these structures to slip in the observed direction, we find that the expected value for the orientation of the maximum compressive stress is 13° off the normal to the Calaveras Fault (Figure 11b). The skewed probability density function is obtained by bootstrap analysis perturbing the input data within the errors and over the range of inversion parameters. The 95% confidence interval for this orientation is [7 16] degrees. This is a very high angle, much higher than would be expected based on laboratory derived values of the coefficient of friction [*Byerlee*, 1978]. An effective coefficient of friction of 0.1, or alternately high pore pressure, was necessary to satisfy the known slip directions and generate traction on the faults sufficient for slip. Our results support the conclusion of high-angle maximum compressive stress of *Townend and Zoback* [2001] in contrast to the stress rotation reported for the San Andreas fault in southern California [*Hardebeck and Hauksson*, 1999] and thus has very different implications for the origin of weak faults. In particular, the wide zone of high fluid pressure and low effective normal stress proposed for the southern San Andreas Fault, does not appear applicable to our data set for the Calaveras Fault.

[46] Previous investigators have obtained similar results for a high-angle, maximum compressive stress orientation in this same region because the areas of the inversion included mechanisms from the secondary faulting structures we have analyzed [*Oppenheimer et al.*, 1988; *Zoback et al.*, 1987]. Our work is distinguished from these earlier studies in that the precise relative event locations allow us to resolve these secondary faults as active structures that reach

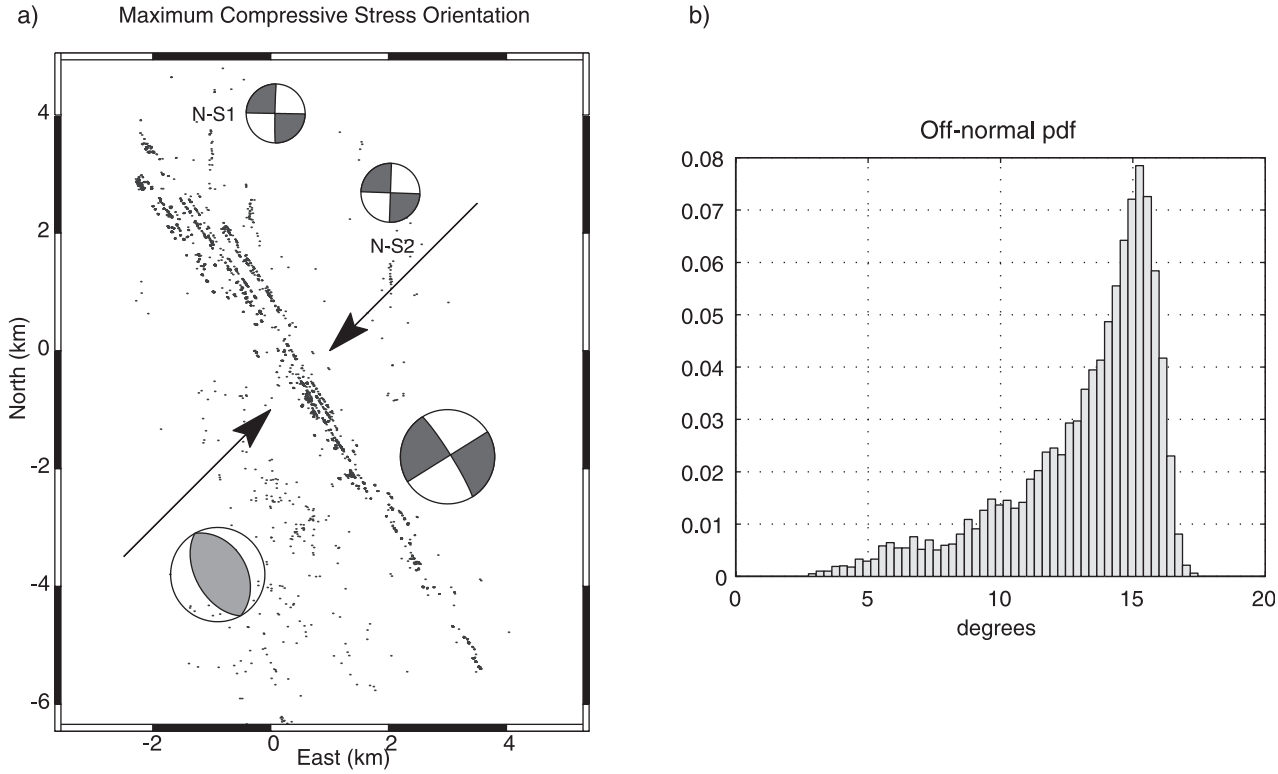

Figure 11. (a) Composite focal mechanisms of Calaveras Fault and off-fault structures. The maximum compressive stress is computed to be at a high angle to the fault. (b) Bootstrap error analysis for the inversion produces a skewed distribution for the orientation angle compared to the fault normal. The expected value is 13° with a 95% confidence interval from [7 16] degrees inclusive.

nearly to the Calaveras Fault itself and hence to constrain the lack of stress rotation in the near field.

9. Conclusions

[47] Through applying the double-difference location method to cross-correlation derived differential arrival times, we are able to reduce errors in location for seismicity on and near the Calaveras Fault by more than an order of magnitude. This reveals details of fault zone structure and seismicity that were previously unknown. We find that the relocated seismicity is highly organized both in time and space, which was previously obscured by location errors. The Calaveras Fault has many repeating earthquakes and subhorizontal streaks of earthquakes. Holes in the seismicity appear to be the locus of slip in occasional larger earthquakes. The Calaveras Fault at depth is extremely thin, with an average upper bound on fault zone width of 75 m. The sense of slip on subsidiary fault structures that reach within a few hundred meters of the Calaveras Fault indicate that the maximum compressive stress is at a high angle to the Calaveras Fault, only 13° from the fault normal vector, supporting previous interpretations that this fault is weak. The relocation technique we have used to study the behavior of the Calaveras Fault opens a new window on the earthquake source. By resolving the structure of seismicity at smaller length scales, we can address many important problems in earthquake mechanics.

Table 2. Fault Planes Used for Stress Inversion

Fault	Dip Direction	Dip Angle	Rake Angle
Calaveras	58°	84°	180°
Thrust	61°	33°	90°
N-S1	91°	88°	180°
N-S2	92°	89°	180°

[48] **Acknowledgments.** We thank Eva Zanzerkia for her comments on and help with aspects of the relocation work. Helpful discussions and reviews were provided from Andy Michael, Allan Rubin, John Townend, Mark Zoback, Paul Segall, David Pollard, Roland Bürgmann, Keith Richards-Dinger, and Jeff McGuire. We thank the NCSN and NCEDC for the ease of retrieving seismograms from their archive and availability of data over the Internet. This work was supported by NSF grant EAR-9725238 and EAR-0074084.

References

Angelier, J., Determination of the mean principal directions of stresses for a given fault population, *Tectonophysics*, *56*, T17–T26, 1979.

Bakun, W. H., M. M. Clark, R. S. Cockerham, W. L. Ellsworth, A. G. Lindh, W. H. Prescott, A. F. Shakal, and P. Spudich, The 1984 Morgan Hill, California, earthquake, *Science*, *225*, 288–291, 1984.

Bakun, W. H., G. C. P. King, and R. S. Cockerham, Seismic slip, aseisimic slip, and the mechanics of repeating earthquakes on the Calaveras Fault, California, in *Earthquake Source Mechanics*, *Geophys. Monogr. Ser.*, vol. 37, edited by S. Das, J. Boatright, and C. H. Scholz, pp. 195–207, AGU, Washington, D. C., 1986.

Beeler, N. M., D. A. Lockner, and S. H. Hickman, A simple stick-slip and creep slip model for repeating earthquakes and its implication for micro-earthquakes at Parkfield, *Bull. Seismol. Soc. Am.*, *91*, 1797–1804, 2001.

Beroza, G. C., and P. Spudich, Linearized inversion for fault rupture behavior; application to the 1984 Morgan Hill, California, earthquake, *J. Geophys. Res.*, *93*, 6275–6296, 1988.

Byerlee, J. D., Friction of rocks, *Pure Appl. Geophys.*, *116*, 615–629, 1978.

Deichmann, N., and M. Garcia-Fernandez, Rupture geometry from high-precision relative hypocentre locations of microearthquake ruptures, *Geophys. J. Int.*, *110*, 501–517, 1992.

Ellsworth, W. L., Characteristic earthquakes and long-term earthquake forecasts: Implications of central California seismicity, in *Urban Disaster Mitigation*, edited by F. Y. Cheng and M. S. Sheu, pp. 1–14, Elsevier Sci., New York, 1995.

Felzer, K. R., and G. C. Beroza, Deep structure of a fault discontinuity, *Geophys. Res. Lett.*, *26*, 2121–2124, 1999.

Fréchet, J., Sismogenèse et doublets sismiques, thèse d'etat, 206 pp., Univ. Sci. et Méd. de Grenoble, Grenoble, France, 1985.

Geiger, L., Herdbestimmung bei Erdbeben aus den Ankunftszeiten, *K. Ges. Wiss. Goett.*, *4*, 331–349, 1910.

Gillard, D., A. M. Rubin, and P. Okubo, Highly concentrated seismicity caused by deformation of Kilauea's deep magma system, *Nature*, *384*, 343–346, 1996.

Got, J.-L., J. Fréchet, and F. W. Klein, Deep fault plane geometry inferred from multiplet relative relocation beneath the south flank of Kilauea, *J. Geophys. Res.*, *99*, 15,375–15,386, 1994.

Hardebeck, J. L., and E. Hauksson, Role of fluids in faulting inferred from stress field signatures, *Science*, *285*, 236–239, 1999.

Hartzell, S. H., and T. H. Heaton, Rupture history of the 1984 Morgan Hill, California, earthquake from the inversion of strong motion records, *Bull. Seismol. Soc. Am.*, *76*, 649–674, 1986.

Li, Y.-G., P. C. Leary, K. Aki, and P. Malin, Seismic trapped modes in the Oroville and San Andreas Fault zones, *Science*, *249*, 763–766, 1990.

Li, Y.-G., J. E. Vidale, K. Aki, C. J. Marone, and W. H. K. Lee, Fine structure of the Landers fault zone; segmentation and the rupture process, *Science*, *265*, 367–370, 1994.

Li, Y.-G., K. Aki, and F. L. Vernon, San Jacinto fault zone guided waves; a discrimination for recently active fault strands near Anza, California, *J. Geophys. Res.*, *102*, 11,689–11,701, 1997.

Li, Y.-G., K. Aki, J. E. Vidale, and M. G. Alvarez, A delineation of the Nojima Fault ruptured in the *M* 7.2 Kobe, Japan, earthquake of 1995 using fault zone trapped waves, *J. Geophys. Res.*, *103*, 74,247–74,263, 1998.

Mendoza, C., and S. H. Hartzell, Aftershock patterns and main shock faulting, *Bull. Seismol. Soc. Am.*, *78*, 1438–1449, 1988.

Michael, A., Effects of three-dimensional velocity structure on the seismicity of the 1984 Morgan Hill, California, aftershock sequence, *Bull. Seismol. Soc. Am.*, *78*, 1199–1221, 1988.

Nadeau, R. M., and L. R. Johnson, Seismological studies at Parkfield, VI, Moment release rates and estimates of source parameters for small repeating earthquakes, *Bull. Seismol. Soc. Am.*, *88*, 790–814, 1998.

Nadeau, R. M., and T. V. McEvilly, Fault slip rates at depth from recurrence intervals of repeating microearthquakes, *Science*, *285*, 718–721, 1999.

Oppenheimer, D. H., P. A. Reasenberg, and R. W. Simpson, Fault plane solutions for the 1984 Morgan Hill, California, earthquake sequence; evidence for the state of stress on the Calaveras Fault, *J. Geophys. Res.*, *93*, 9007–9026, 1988.

Oppenheimer, D. H., W. H. Bakun, and A. G. Lindh, Slip partitioning of the Calaveras Fault, California, and prospects for future earthquakes, *J. Geophys. Res.*, *95*, 8483–8498, 1990.

Poupinet, G., W. L. Ellsworth, and J. Fréchet, Monitoring velocity variations in the crust using earthquake doublets: An application to the Calaveras Fault, California, *J. Geophys. Res.*, *89*, 5719–5731, 1984.

Prescott, W. H., N. E. King, and G. Guohua, Preseismic, coseismic, and postseismic deformation associated with the 1984 Morgan Hill, California, earthquake, in *The 1984 Morgan Hill, CA earthquake*, edited by J. H. Bennett and R. W. Sherburne, *Spec. Publ. Calif. Div. Mines Geol.*, *68*, 137–148, 1984.

Radbruch-Hall, D. H., Map showing recently active breaks along the Hayward Fault zone and the southern part of the Calaveras Fault zone, California, *U. S. Geol. Surv. Misc. Invest.*, *I-813*, 1974.

Rubin, A. M., Aftershocks of microearthquakes as probes of the mechanics of rupture, *J. Geophys. Res.*, *107*(B7), 2142, doi:10.1029/2001JB000496, 2002.

Rubin, A. M., D. Gillard, and J.-L. Got, Streaks of microearthquakes along creeping faults, *Nature*, *400*, 635–641, 1999.

Sammis, C. G., and J. R. Rice, Repeating earthquakes as low-stress drop events at a border between locked and creeping fault patches, *Bull. Seismol. Soc. Am.*, *91*, 532–537, 2001.

Schaff, D. P., 4D high resolution seismology: Repeating events and large scale relocation, Ph.D. thesis, 115 pp., Stanford Univ., Stanford, Calif., 2001.

Schaff, D. P., G. C. Beroza, and B. E. Shaw, Postseismic response of repeating aftershocks, *Geophys. Res. Lett.*, *25*, 4549–4552, 1998.

Sibson, R. H., Roughness at the base of the seismogenic zone: Contributing factors, *J. Geophys. Res.*, *89*, 5791–5799, 1984.

Townend, J., and M. D. Zoback, Implications of earthquake focal mechanisms for the frictional strength of the San Andreas Fault system. in *The Nature and Tectonic Significance of Fault Zone Weakening*, edited by R. E. Holdsworth et al., *Geol. Soc. Spec. Publ.*, *186*, 13–21, 2001.

Waldhauser, F., A computer program to compute double-difference hypocenter locations, *U.S. Geol. Surv. Open File Rep., 01-113*, 25 pp., 2001.

Waldhauser, F., and W. L. Ellsworth, A double-difference earthquake location algorithm: Method and application to the northern Hayward Fault, California, *Bull. Seismol. Soc. Am.*, *90*, 1353–1368, 2000.

Waldhauser, F., and W. L. Ellsworth, Fault structure and mechanics of the Hayward Fault, California, from double-difference earthquake locations, *J. Geophys. Res.*, *107*(B3), 2054, doi:10.1029/2000JB000084, 2002.

Waldhauser, F., W. L. Ellsworth, and A. Cole, Slip-parallel seismic lineations along the northern Hayward Fault, California, *Geophys. Res. Lett.*, *26*, 3525–3528, 1999.

Working Group on California Earthquake Probabilities (WGCEP), Earthquake probabilities in the San Francisco Bay region: 2000 to 2030—A summary of findings, online version 1.0, *U.S. Geol. Surv. Open file Rep., 99-517*, 60 pp., 1999.

Zoback, M. D., et al., New evidence on the state of stress of the San Andreas Fault system, *Science*, *238*, 1105–1111, 1987.

G. C. Beroza and G. H. R. Bokelmann, Department of Geophysics, Stanford, CA 94305-2215, USA. (beroza@pangea.stanford.edu; schaff@geo.stanford.edu)

W. L. Ellsworth, U.S. Geological Survey, 345 Middlefield Road, MS 977, Menlo Park, CA 94025-3591, USA. (ellsworth@usgs.gov)

D. P. Schaff and F. Waldhauser, Lamont-Doherty Earth Observatory, Route 9W, Palisades, NY 10964-1000, USA. (dschaff@ldeo.columbia.edu; felixw@ldeo.columbia.edu)